Pergamon

*Int. J. Heat Mass Transfer.* Vol. 39, No. 11, pp. 2253–2266, 1996

0017–9310/96 $15.00 + 0.00

0017–9310(95)00333–9

# Convective heat transfer in rotating ribbed tubes

W. D. MORRIS† and K. FARHADI RAHMAT-ABADI‡

† Department of Mechanical Engineering, University College of Swansea, Singleton Park, Swansea SA2 8PP, U.K.

‡ AEOI, Nuclear Research Centre, PO Box 11365-8486, Tehran, Iran

(*Received* 25 *May* 1994 *and in final form* 17 *August* 1995)

**Abstract**—This paper describes an experimental investigation of the effect of internal ribs and orthogonal-mode rotation on forced convection in circular tubes. Depending on the rib geometry, heat transfer is improved by up to threefold in comparison with a smooth-walled circular tube at zero rotation. Results are presented for three rib geometries which are typical of those used in turbine rotor blade cooling channels. With rotation Coriolis-induced secondary flows increase heat transfer on the trailing edge of the tube in comparison to the leading edge. The effect of centripetal buoyancy is also investigated and the combined effect of Coriolis forces and buoyancy is demonstrated. Copyright © 1996 Elsevier Science Ltd.

## 1. INTRODUCTION

Prediction of heat transfer inside the cooling channels of high performance aero-gas turbine rotor blades remains a task of the utmost difficulty, despite the fact that air cooling of these components has been a standard design feature for over thirty years. The technical difficulty arises for two main reasons.

Firstly, the cooling channels are often fitted with ribs, fins, pins, etc. which induce three-dimensionality into the flow field. Also the coolant channels are often connected in a multi-pass manner so that coolant can flow in a radially outward or inward direction as it progresses through the blade. At the channel interconnections, bends create additional complexities in the flow which are not easy to predict with certainty. The second difficulty relates to the fact that the coolant rotates with the channel, thus experiencing Coriolis and centripetal forces which change the nature of the flow and hence the internal heat transfer.

Coriolis forces create secondary flow in the channels, the effect of which is to induce relatively better cooling on the trailing surface of the channel compared to that on the leading surface. The interaction of centripetal forces with coolant density variations gives rise to a buoyancy effect which further modifies the flow and heat transfer.

The influence of rotation on flow and heat transfer in smooth walled ducts has been extensively studied in Europe and the U.S.A. in recent years and refs. [1]–[26] cite the main results arising from these investigations. Less work has been done on the combined effect of surface heat transfer augmentation devices and rotation in the rotor blade cooling application, see for example refs. [27]–[30]. Accordingly the present paper presents the results of an experimental study which addresses this problem for the case of tubes fitted with internal circumferential ribs.

## 2. DESCRIPTION OF THE FLOW GEOMETRY

The ribbed geometry studied involved a circular tube fitted with circumferential ribs as indicated in Fig. 1. The geometric features of a given test channel may be described in non-dimensional terms using a suitable dimensional scaling factor. Thus if the pitch, $p$, is selected for scaling we can describe the test sections via the following dimensionless groups,

$$\Pi_1 = p/D \quad \text{(pitch : plain bore diameter ratio)} \quad (1)$$

$$\Pi_2 = d/p \quad \text{(bore diameter at rib : pitch ratio)} \quad (2)$$

$$\Pi_3 = a/p$$

$$\text{(axial location of first and last rib : pitch ratio)} \quad (3)$$

$$\Pi_4 = b/p \quad \text{(rib land : pitch ratio).} \quad (4)$$

Three test section geometries were actually tested with each channel fitted with five sets of ribs. Thus the overall length of the test sections may be scaled relative to the pitch to give

$$\Pi_5 = L/p = 2(\Pi_3 + 2). \quad (5)$$

These five $\Pi$-groups have been used to define the main features of the three test sections in this paper. There are instances where alternative descriptors may be convenient. For example the axial location downstream of entry to the test section may be defined in terms of the equivalent number of plain bore diameters. Similarly the blockage effect, $\Pi_6$, due to the presence of a rib may be defined as the ratio of the axially viewed area of the rib to the plain bore diameter of the channel, so that

## NOMENCLATURE

| | |
|---|---|
| $a$ | location of first rib from entry station and location of last rib from exit station |
| $b$ | rib land |
| $Bu$ | buoyancy parameter |
| $d$ | bore diameter at a rib location |
| $D$ | plain bore diameter |
| $H$ | eccentricity of entry station |
| $p$ | rib pitch |
| $Nu$ | Nusselt number |
| $Pr$ | Prandtl number |
| $q$ | heat flux |
| $Ra$ | rotational Rayleigh number |
| $Re$ | Reynolds number |
| $Ro$ | Rossby number |
| $T$ | temperature |
| $w$ | mean axial velocity |
| $z$ | axial location relative to entry station. |

Greek symbols

| | |
|---|---|
| $\beta$ | volume expansion coefficient |
| $\varepsilon$ | eccentricity parameter |
| $\nu$ | kinematic viscosity |
| $\Pi_1$ | pitch : plain bore diameter ratio |
| $\Pi_2$ | bore diameter at rib : pitch ratio |
| $\Pi_3$ | axial location of first and last rib : pitch ratio |
| $\Pi_4$ | rib land : pitch ratio |
| $\Pi_5$ | overall length : pitch ratio |
| $\Pi_6$ | blockage ratio |
| $\phi$ | function |
| $\Psi$ | function |
| $\Omega$ | angular velocity. |

Subscripts

| | |
|---|---|
| b | fluid bulk value |
| o | non-rotational value |
| R | rotational value |
| w | wall value |
| z | axial location value |
| $\infty$ | fully developed non-rotational value. |

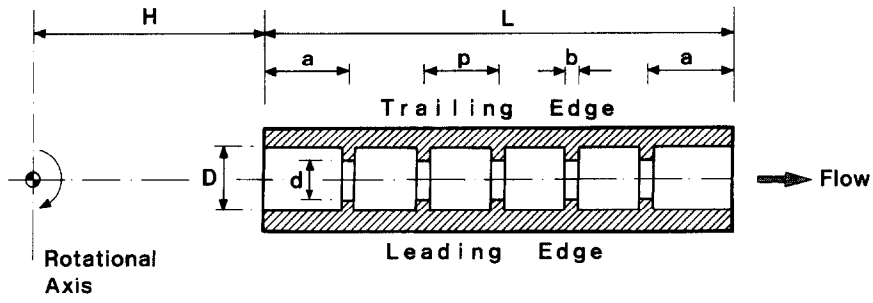


**Plain bore diameter - D** **Rib land - b**
**Rib pitch - p** **Location of first rib from entry - a**
**Bore at rib location - d** **Location of final rib from exit - a**

Fig. 1. Description of basic flow geometry.

$$\Pi_6 = 1-(d/D)^2 = 1-(\Pi_2 \cdot \Pi_1)^2 \quad \text{(blockage ratio)}. \tag{6}$$

Equations (1)–(6) describe the test section geometry itself. One further geometric parameter is needed to describe the location of the section relative to the axis of rotation. An eccentricity parameter, $\varepsilon$, defined as

$$\varepsilon = H/D \tag{7}$$

is convenient, where $H$ is the eccentricity of the entry plane of the test section in relation to the axis of rotation, as indicated in Fig. 1.

The range of geometric parameters studied in this paper reflects values typically used for rotor blade cooling. Preliminary results obtained with one of these test sections have been reported by Morris and Salemi [30] and the work presented in this paper is an extension which includes a fuller study of combined geometric and rotational effects.

### 3. APPARATUS

To investigate the individual effect of each non-dimensional geometric variable would require a vast amount of experimentation. Thus, in consultation with the funding sponsors, three geometric configurations were selected for an initial programme of fundamental work. Each test section constructed had five sets of equispaced ribs and the absolute dimensional features of these test sections are given in Table 1 with the corresponding non-dimensional geometric parameters given in Table 2.

Table 1. Dimensional details of test sections

| Dimensions [mm] | Test section A | Test section B | Test section C |
|---|---|---|---|
| Plain bore diameter | 10.00 | 10.00 | 10.00 |
| Rib pitch | 20.00 | 15.00 | 10.00 |
| Bore at rib location | 6.00 | 7.00 | 8.00 |
| Rib land | 2.00 | 1.50 | 1.00 |
| Location of first rib from entry | 25.00 | 18.75 | 12.50 |
| Location of final rib from exit | 25.00 | 18.75 | 12.50 |
| Eccentricity of test section inlet | 270 | 270 | 270 |
| Actively heated length | 130.00 | 97.50 | 65.00 |

Table 2. Non-dimensional geometric details of test sections

| Geometric description (expressed as ratios) | Test section A | Test section B | Test section C |
|---|---|---|---|
| Pitch : plain bore ($\Pi_1$) | 2.00 | 1.50 | 1.00 |
| Bore at rib : pitch ($\Pi_2$) | 0.30 | 0.47 | 0.80 |
| First rib location : pitch ($\Pi_3$) | 1.25 | 1.25 | 1.25 |
| Land : pitch ($\Pi_4$) | 0.10 | 0.10 | 0.10 |
| Overall length : pitch ($\Pi_5$) | 6.50 | 6.50 | 6.50 |
| Blockage ($\Pi_6$) | 0.64 | 0.51 | 0.36 |
| Eccentricity : plain bore ($\varepsilon$) | 27.00 | 27.00 | 27.00 |

The basic constructional method adopted was the same for all models, with minor adaptions to suit the actual physical size involved. Test Section A in Table 1 will be described in detail to illustrate these general constructional features.

The construction is depicted in Fig. 2. The test section, (1), was made from machinable ceramic glass having a thermal conductivity of 1.3 W $m^{-1}$ $K^{-1}$. This material was used to minimise the effect of axial conduction along the walls of the test section. This point will be discussed in more detail when the method of data analysis is described in the next section. This ribbed test section had a plain bore diameter of 10 mm and a wall thickness of 1.50 mm, giving an outer diameter of 13.00 mm. Insulating–supporting bushes, (2), (3), (4) and (5), fitted to the ends of the glass test section, permitted support in an aluminium split cylindrical shell casing, (6).

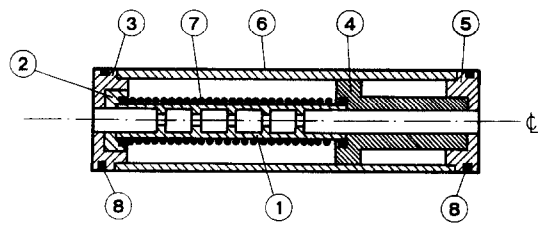


1 Circular sectioned tube
2 Insulated inlet bush
3 Aluminium support bush
4 Insulated exit bush
5 Aluminium support bush
6 Aluminium split case
7 Heating wire
8 "O" ring seals

Fig. 2. Test section construction.

The outer surface of the test section was electrically heated using Nichrome resistance wire, (7), helically wound over the surface. The wire was located in a thread machined on the surface with the depth of thread corresponding to the nominal wire diameter of 0.50 mm. The ends of the heating wire were attached to terminal posts screwed into the inside faces of the insulated bushes (2) and (4). In this way the actively heated length of the test section was 130.00 mm.

The wall temperature of the test section was measured by embedding type-K thermocouples in grooves machined on the outer surface, with the depth arranged to locate the sensing junction 0.5 mm from the inner surface of the plain bore tube. Thermocouples were embedded on the edges of the test section which corresponded to the leading and trailing edges

when rotating and at the nominal rib and mid rib locations. Thermocouples were also embedded in the wall at locations very close to the inlet and exit stations of the test section and at the mid-point of the plain bore section following the final rib. Type-K thermocouples were also used to measure the coolant temperature at the inlet and exit stations of the test section. These were located on the centre line of the ribbed tube. The thermocouple lead off wires and the current carrying leads for the heating wire were taken from the test section via holes machined in the bushes (4) and (5).

This self contained test module fitted into an air delivery plenum chamber which formed part of the rotating test facility to be described below. Air leakage from the plenum was inhibited by means of two 'O' ring seals, (8), fitted to the inlet and exit end of the casing. External heat loss was minimised by back filling the space between the surface of the heater section and the inner surface of the casing with Fiberfax insulation.

The schematics of the rotating test facility used is shown in Fig. 3. An air delivery plenum, (1), which carries the instrumented test module, is fitted to a shaft, (2), which is supported between two bearings, (3). This built up rotor was driven by an electric motor, (4), using pulley drive, (5). A magnetically held face seal (6) was used to permit relative motion between the right hand end of the rotor shaft (as viewed in Fig. 3) whilst preserving a leak proof seal for the passage of air into the bored out end of the shaft which communicated with the air delivery plenum chamber. Each test section had a standardised exterior and could be fitted into the outer end of the plenum chamber, (1), being held in place by means of an internal spacer and a threaded end cap, (7).

Pressurised dry and oil free air was fed to the inlet side of the rotary seal and hence through the test section itself before being vented to atmosphere. The air flow was measured using an Annubar differential pressure flow meter in the upstream pipe line with precise flow settings controlled by means of a control valve.

Electrical power for the heater was fed to the test section via a two-channel power slip ring, (8), with power control effected using a Variac transformer. Heater power was measured using a conventional wattmeter. Thermocouple signals were monitored using a Schlumberger Orion data acquisition system via a 60 channel silver/silver–graphite instrumentation slip ring assembly, (9), and the rotor speed was monitored using a magnetic encoder and electronic timer counter.

## 4. METHOD OF DATA EVALUATION

Each test section was subjected to the same experimental programme. This involved the measurement of local heat transfer coefficients at the rib and mid-rib locations on the leading and trailing edges. Four Reynolds number values were used and, at each of these, tests were undertaken at four values of rotational speed. The Reynolds numbers, evaluated at the inlet to the test section using the inlet temperature for the determination of properties, were nominally 15000, 20000, 25000 and 30000, respectively and the rotational speeds were 0, 1000, 2000 and 2700 rev $min^{-1}$, respectively. At each Reynolds number–speed combination tests were undertaken at five different heater powers, giving a total of 80 experiments for each section. The strategy underlying this test procedure was as follows.

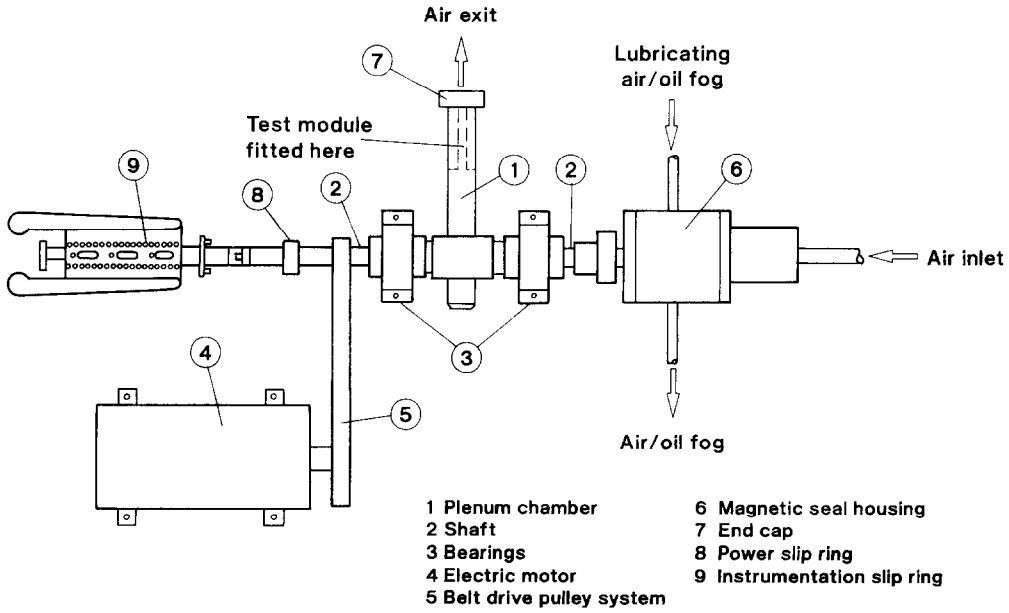


Fig. 3. Rotating test facility.

For a given geometry the local heat transfer will be influenced by the zero speed forced convection associated with the through flow Reynolds number, $Re$. With rotation Coriolis and buoyancy forces further complicate the problem. It may be demonstrated, see Morris [11], that the Coriolis effect may be characterised using the Rossby, $Ro$, number defined as

$$Ro = w/\Omega D \tag{8}$$

where all symbols are as defined in the Nomenclature.

With terrestrial free convection it is customary to use a Rayleigh number, $Ra$, to quantify the buoyancy effect using the earth's gravitational acceleration as the body force term. This has led some workers in the field of rotational heat transfer to adopt a similar non-dimensional group, but using a convenient measure of the centripetal acceleration to replace gravity. For the present geometry, we could use a rotational Rayleigh number defined as

$$Ra = H\Omega^2 D^3 \beta (T_w - T_b) Pr/v^2. \tag{9}$$

However this parameter may be re-written in terms of the Reynolds and Rossby numbers as

$$Ra = (H/d)(Re/Ro)^2 Pr\beta(T_w - T_b). \tag{10}$$

Since the Reynolds and Rossby numbers characterise the zero speed forced convection and Coriolis effects in their own right, the influence of buoyancy may be described in terms of the product of the eccentricity ratio, $\varepsilon$, and a buoyancy parameter, $Bu$, defined as

$$Bu = \beta(T_{w,z} - T_{b,z}). \tag{11}$$

If the local Nusselt number, $Nu_{R,z}$, is defined in the usual manner at a distance, $z$, from the entry plane, as

$$Nu_{R,z} = qD/k(T_{w,z} - T_{b,z}) \tag{12}$$

then we might expect the overall effect of rib geometry, coolant flow rate and rotation on local heat transfer to conform to an equation of form

$$Nu_{R,z} = \Phi(Re, Ro, \varepsilon Bu, Pr, z/D, \Pi_1, \Pi_2, \Pi_3, \Pi_4) \tag{13}$$

where $\Phi$ is some function of the variables enclosed in the brackets.

Prior to conducting the experimental programme itself a series of heat loss calibration tests were undertaken to determine the external heat loss characteristics of each test section assembly at all rotational speeds used. Using the loss characteristics it was possible to calculate the variation of heat flux to the coolant along the test section. In turn an enthalpy balance permitted the variation of fluid bulk temperature to be determined. Generally, comparison of the measured fluid exit bulk temperature from the test section with the calculated value suggested that stray heat losses were of the order of 10% of the total heating power supplied to the test sections. Local Nusselt numbers at the nominal rib and mid-rib locations were subsequently evaluated for the leading and trailing edges using equation (12). In this respect the wall temperatures used were corrected to the plain bore effective surface locations. Further details of the procedure are given by Morris and Salemi [30].

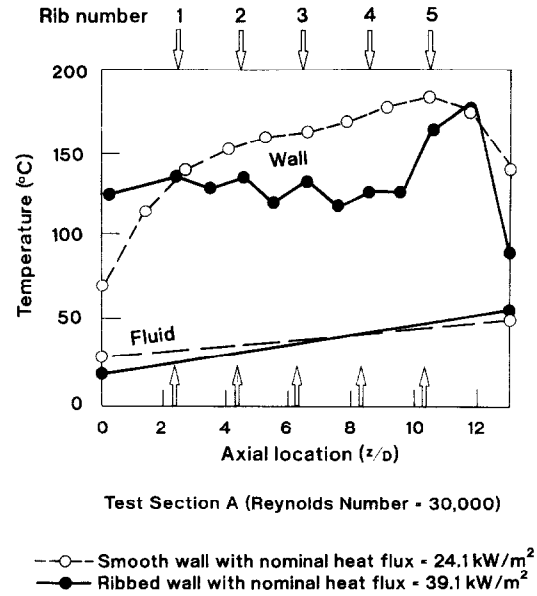


Fig. 4. Typical effect of rib geometry on measured wall temperature distributions with no rotation.

## 5. RESULTS AND DISCUSSION

### 5.1. *Results obtained with zero rotation*

Figure 4 shows the typical measured streamwise variation of wall temperature. In this example Test Section A is used for convenience of illustration since direct comparison with the results of Morris and Salemi [26] may be made for a smooth-walled tube having identical overall dimensions. The trends depicted were similar to those obtained with all other test sections over the entire range of Reynolds numbers and heat flux settings. The temperature measurements obtained on the leading and trailing edges were in close agreement as expected with the axisymmetric zero speed set of tests.

In Fig. 4 the smooth wall data, from Morris and Salemi [26], is shown as a reference state. This follows the well known distribution associated with a basically uniform heat flux thermal boundary condition. As the hydrodynamic and thermal boundary layers develop simultaneously we note the increasing wall temperature in the flow direction. The wall temperature approaches a uniform gradient as the flow develops, with an "end effect" inducing a fall in temperature at the exit end of the test section.

The following two points are worthy of note for the ribbed data. Firstly, instead of the smoothly varying temperature typical of the smooth wall situation, the temperature tends to follow a "saw tooth" variation

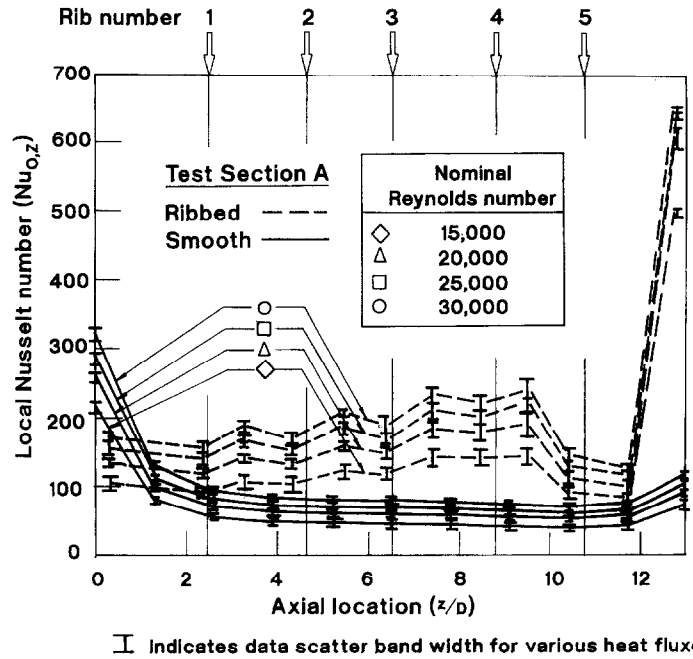


Fig. 5. Typical effect of ribs on measured local Nusselt number distribution with no rotation.

as the flow negotiates the alternate rib and mid-rib positions. The higher points on this "saw tooth" ripple occurred at the rib locations suggesting relatively better heat transfer at the mid-rib locations, where reattachment zones will be occurring. These representative curves also demonstrate the improved heat transfer generally obtained with the ribs fitted since the nominal heat flux (39.1 kW $m^{-2}$) conforming to the ribbed data is approximately 62% greater than that corresponding to the smooth walled tube whilst the wall temperature with ribs fitted is dramatically reduced over the major part of the heated test section. Detailed examination of the measured temperature profiles obtained with Test Sections B and C were similar to those obtained with Test Section A, but the severity of the temperature ripple tended to reduce systematically with reductions in the blockage ratio.

Local Nusselt numbers, based on the temperature shown in Fig. 4, were evaluated in accordance with the definition described in Section 4 and resulting variations are shown in Fig. 5. Data covering the full range of Reynolds numbers tested are shown in this figure. The "saw tooth" wall temperature ripple discussed above is reflected in the local Nusselt number results and the enhanced heat transfer obtained with ribs fitted is clearly evident. The pattern of streamwise local Nusselt number obtained with all three ribbed geometries was similar. The end loss effect common with forced convection experimentation is also present with the ribbed tubes and for this reason only the results of the first four ribs will be considered for more detailed analysis.

Figure 6 compares the relative enhancement in heat transfer for each of the three ribbed geometries. For each of the four Reynolds numbers tested, the local heat transfer has been plotted against the axial location downstream of entry based on an equivalent plain bore diameter scale. Also indicated in this diagram, for comparative purposes, is the Dittus–Boelter [31] value for developed flow in a smooth-walled tube. The following features should be noted. With the exception of the initial entrance region, say up to the first rib location, there was a systematic trend as regards the three test sections. Test Section A produced the highest relative heat transfer followed by Test Section B and the Test Section C. Because the pitch : plain bore diameter ratio and the blockage ratio were simultaneously changing as one compares the results of the three test sections, it is not possible to evaluate the individual effect of these two geometric variables precisely with the present data. However, with progressively increasing pitch : plain bore diameter ratios one would expect the larger sections of plain bore tube in ribs to reduce the overall influence of this parameter. Since Test Section A involves the largest pitch : plain bore diameter ratio and also the greatest blockage ratio, there is a suggestion that the blockage ratio is an important performance parameter. The heat transfer enhancement is progressively better as the penetration of the rib into the core flow region increases.

Figure 7 attempts to quantify the relative enhancement in heat transfer likely to be achieved by the incorporation of ribs. In this figure, which is not strictly speaking a graphical trend for reasons explained below, the rib cell between ribs numbered 3 and 4 is studied in more detail. As a measure of heat transfer enhancement, the local Nusselt numbers obtained with ribs fitted have been scaled relative to the fully developed Nusselt number, $Nu_{0,\infty}$, for smooth-walled

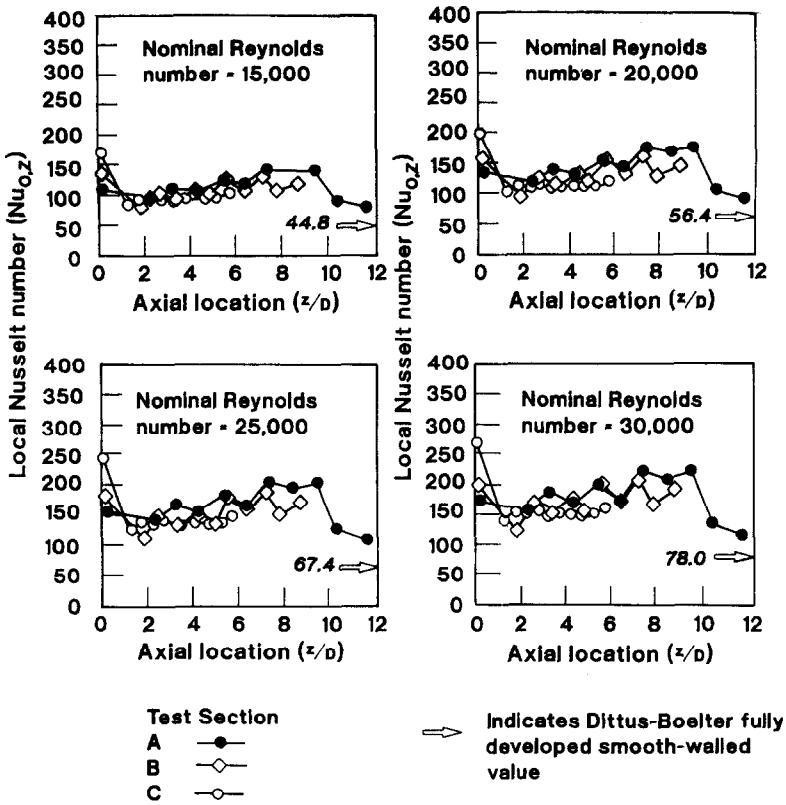


Fig. 6. Effect of rib geometry on local heat transfer for a range of Reynolds numbers with no rotation.

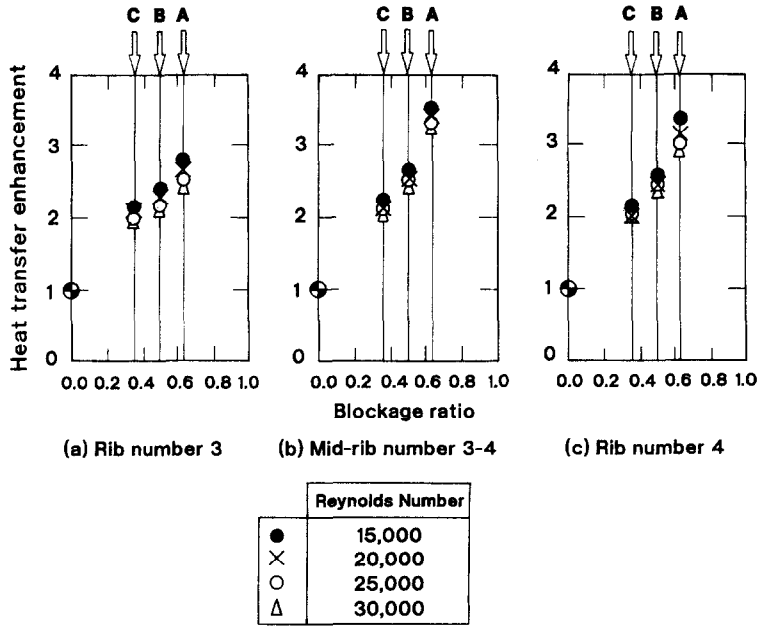


Fig. 7. Typical levels of heat transfer enhancement relative to smooth-walled, fully developed forced convection.

forced convection as given by the Dittus–Boelter [31] correlation. In this respect, for a relatively invariant value of Prandtl number over the range of temperatures covered by this investigation, we may use the following result for the determination of this fully developed scaling value.

$$Nu_{0,\infty} = 0.02Re^{0.8}. \tag{14}$$

It was mentioned above that the blockage ratio and the pitch : plain bore diameter changed when we changed Test Sections from A to B to C. Thus in Fig. 7, where the relative heat transfer enhancement is

plotted against the blockage ratio, it should be noted that the data sets for Test Sections A, B and C do involve a pitch : plain bore diameter ratio as well. Nevertheless some interesting trends may be observed.

The heat transfer enhancement for each test section is Reynolds number dependent with the highest enhancements occurring at the lowest Reynolds number values. Depending on the actual rib geometry heat transfer enhancement up to three times that corresponding to smooth walled fully developed forced convection may be obtained and this level of improvement can be maintained over virtually the entire length of the channel.

Although the pitch : plain bore diameter ratio varies as well as the blockage ratio in the selection of geometries studied in this report, the test sections A, B and C have an almost linear relationship between these parameters given by

$$\Pi_1 = 3.571\Pi_7 - 0.2857. \quad (15)$$

Thus Fig. 7 can be used to estimate the individual effects of these two geometric parameters provided equation (15) is used as a control. Obviously more experimentation is necessary to completely define the independent influences of these geometric features.

These experimental results will be treated as a reference base to examine the combined influence of ribs and rotation in the next section of this paper.

### 5.2. *Results obtained with rotation*

When the programme of experiments was repeated with rotation, significant changes in the distribution of local heat transfer along the channels occurred in relation to the non-rotational forced convection situation. These changes were consistent with the presence of strong Coriolis-driven secondary flows and also a centripetal buoyancy interaction.

Figure 8 shows measured wall temperature distributions along each of the test sections with the maximum rotational speed of 2700 rev min$^{-1}$ and the highest Reynolds number of 30 000, which corresponds to a nominal Rossby number of 18.27. In each case the temperatures on the leading and trailing edges of the channels are shown and significant separation is evident. This separation is consistent with the presence of a Coriolis-driven secondary flow as described in the introductory section of this paper. In all cases the trailing edge was operating at a lower temperature compared to its leading counterpart as predicted by the movement of relatively cool core region flow from the centre of the channel towards the trailing edge. The "saw tooth" downstream temperature distribution detected with zero rotation (see Fig. 4) was still evident with rotation. In this respect the leading and trailing edges exhibit similar trends with the temperature peaks located in the region of the individual ribs. Again the severity of the "saw tooth" effect was less marked with Test Section C which has the least blockage effect The main feature which is immediately obvious from this representation of unprocessed raw data is that far better cooling is being achieved on the trailing edge of the channel.

Figure 9 shows a selection of local Nusselt number distributions for each test section. In this figure the lowest and highest Reynolds number values tested are shown by way of illustration. Also included in this figure are the Rossby numbers and buoyancy parameters corresponding the arithmetic mean of all axial measurement points. Note that, in any individual test run, these values vary along the duct. The trends obviously reflect the temperature trends presented in the previous figure, with the measured Nusselt numbers noticeably higher on the trailing edge. The relative difference in heat transfer on the leading and trailing surfaces may be explained in terms of the Coriolis-driven secondary flow field. Again, as with the non-rotational case, the heat transfer is relatively higher in the mid-rib locations where the benefits of re-attachment zones are still seemingly evident even with rotation.

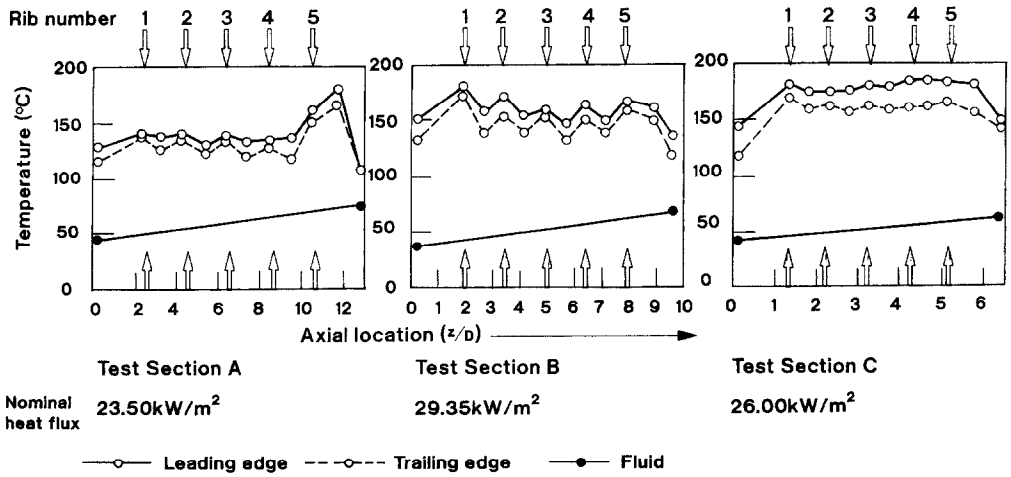


Fig. 8. Typical effect of rotation on measured wall temperature distributions.

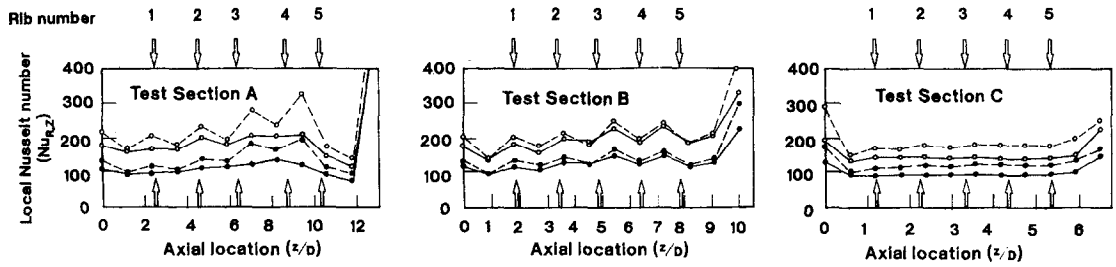


| Test Section | | Nominal Reynolds number | Nominal Rossby number | Average heat flux (kW/m²) | Average Bu on leading edge | Average Bu on trailing edge |
|---|---|---|---|---|---|---|
| A | • | 15,000 | 10.50 | 33.2 | 0.2492 | 0.2129 |
| | ○ | 30,000 | 18.27 | 49.6 | 0.2359 | 0.1917 |
| B | • | 15,000 | 10.50 | 31.9 | 0.3209 | 0.2875 |
| | ○ | 30,000 | 18.27 | 46.8 | 0.3358 | 0.3099 |
| C | • | 15,000 | 10.50 | 30.1 | 0.3562 | 0.3365 |
| | ○ | 30,000 | 18.27 | 44.1 | 0.3690 | 0.3564 |

Fig. 9. Typical effect of rotation on local Nusselt number distributions.

Detailed examination of the experiments undertaken at fixed nominal Rossby and Reynolds numbers, but with varying heat fluxes, demonstrated that there was a noticeable heat flux sensitivity to the distribution of Nusselt number on both the leading and trailing edges. With normal forced convection such sensitivity should be suppressed by the normal process of non-dimensionalisation. Figure 10 illustrates this heat flux sensitivity on the leading edge for the case of Test Section B at the highest rotational speed (2700 rev $min^{-1}$) tested and the same two Reynolds number values as used in Fig. 9. The corresponding nominal Rossby numbers are also shown in the figure.

A heat flux sensitivity is clearly consistent with a centripetal buoyancy effect and it was demonstrated earlier that this could be characterised in these rotational duct flow situations by means of the buoyancy parameter, $Bu$, involving the product of the coolant volume expansion coefficient and a representation of the wall to coolant bulk temperature difference. For this reason the heat flux lines in Fig. 10 have been flagged using the buoyancy parameter evaluated at the mid-rib position between the third and fourth rib. The important point to note is that the local Nusselt number on the leading edge increases with increases in the buoyancy parameter. This is consistent with the work on smooth-walled tubes reported by Morris and Salemi [26] and Wagner *et al.* [19, 23]. Note the important point that the strategy of the experimental programme controlled the Rossby and Reynolds numbers to be within 1% of their nominal values, whilst the heat flux was varied for each batch of tests. Thus in Fig. 10 only the buoyancy is significantly varying. Similar results were found for the trailing edge.

Equation (13), when applied to a specific axial location in a specific rotating ribbed geometry, suggests that the local Nusselt number will be functionally related to the Reynolds number, the Rossby number and the product of the eccentricity parameter and the buoyancy parameter. This assumes that variations in the Prandtl number of the coolant may be ignored and this is a valid assumption over the range of temperatures encountered in the present experimental programme. Because the default version of this functional relationship must conform to the non-rotational case, we may expect the link between the heat transfer, flow field and rotation to have the mathematical form (for both leading and trailing edges)

$$Nu_{R,z} = Nu_{0,z} + \Psi(Re, Ro, \varepsilon Bu) \tag{16}$$

where $\Psi$ is an unknown function. We may rewrite equation (16) as

$$Nu_{R,z}/Nu_{0,z} = 1 + \Psi(Re, Ro, \varepsilon Bu)/Nu_{0,z}. \tag{17}$$

Morris and Salemi [26] attempted to uncouple the combined effect of Coriolis forces and centripetal buoyancy for a smooth-walled circular sectioned tube by assuming that

$$\Psi(Re, Ro, Bu)/Nu_{0,z} = \Psi(Bu/Ro) \tag{18}$$

for a given eccentricity.

This assumption was based on an empirical examination of their data for the smooth-walled circular tube and also the smooth-walled square tube data of Wagner *et al.* [19]. Although not perfect, this quotient of the buoyancy parameter and the Rossby number produced a reasonable correlating method for rotational heat transfer data thus giving an independent measure of the effect of both the rotational mechanisms influencing heat transfer.

The downstream location corresponding to the mid-third–fourth rib has been selected for detailed

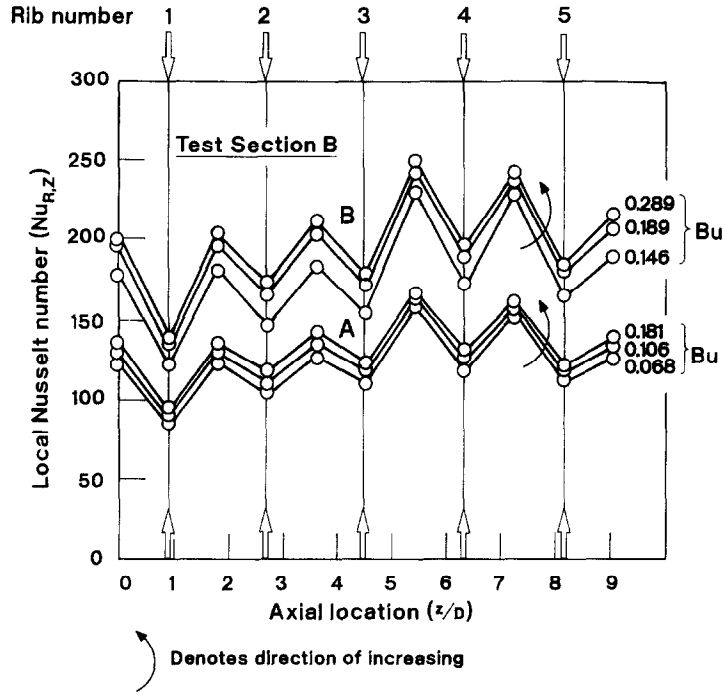


| | Nominal Reynolds number | Nominal Rossby number |
|---|---|---|
| A | 15,000 | 10.50 |
| B | 30,000 | 18.27 |

Fig. 10. Typical effect of centripetal buoyancy on leading edge heat transfer distributions.

examination along the lines suggested by equation (18). Figure 11 shows the ratio of the local Nusselt in relation to that obtained when stationary plotted against the proposed correlating parameter *Bu/Ro*. The results of all rotational speeds and heat fluxes are plotted in this figure. Although there is data scatter present, the combined effect of Coriolis and buoyancy forces is clearly evident on the relative heat transfer. For each test section the heat transfer ratio on the trailing edge increases with increasing values of this combined buoyancy–Coriolis grouping. Over the range of the data covered in the present study trailing edge heat transfer at this location can be up to 30% greater than that expected by ordinary forced convection in the absence of rotation.

It has already been demonstrated that the heat transfer on the leading edge is lower than that on the trailing edge when rotation is present and this is always the case. The influence of the Coriolis secondary flow is a clear reason for this effect. It is interesting, however, to consider the way in which the overall behaviour of leading edge heat transfer relative to the stationary bench mark responds to rotation.

It should be noted that, depending on the value of

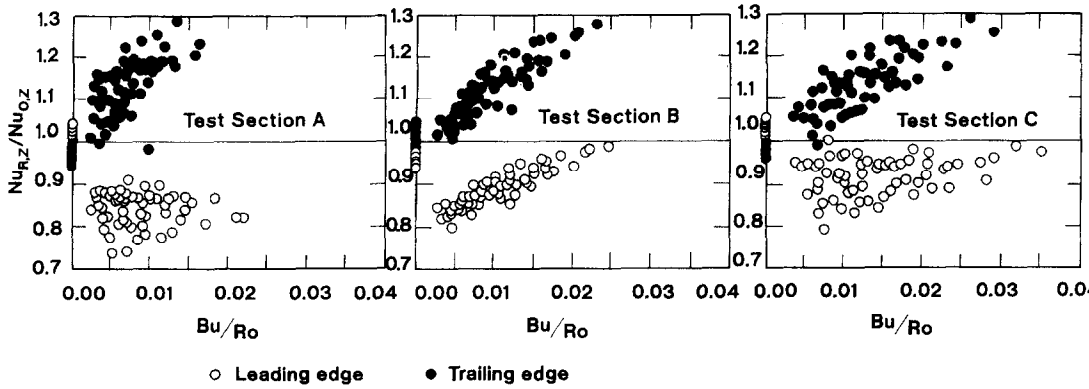


Fig. 11. Combined effect of Coriolis force and buoyancy on heat transfer at mid-rib location numbers 3 and 4.

Table 3. A sample of results at zero speed for test section B

| Axial location $z/D$ | Outer surface heat flux [kW m$^{-2}$] | Wall temperature [°C] | Fluid bulk temperature [°C] | Local Reynolds number | Local Nusselt number |
|---|---|---|---|---|---|
| 0.195 | 30.053 | 119.9245 | 22.15 | 15031.6 | 118.7 |
| 1.853 | 28.797 | 169.2371 | 29.37267 | 14755.4 | 77.83 |
| 2.633 | 29.481 | 142.2666 | 32.62854 | 14635.21 | 100.69 |
| 3.315 | 29.179 | 154.2875 | 35.54295 | 14529.81 | 91.25 |
| 4.095 | 29.666 | 135.0662 | 38.84201 | 14412.92 | 113.42 |
| 4.875 | 29.422 | 144.6498 | 42.19613 | 14296.63 | 104.66 |
| 5.655 | 29.799 | 129.7883 | 45.52267 | 14183.77 | 127.7 |
| 6.338 | 29.422 | 144.8092 | 48.47284 | 14085.67 | 109.4 |
| 7.118 | 29.788 | 130.3635 | 51.79938 | 13977.25 | 134.6 |
| 7.900 | 29.28 | 150.3354 | 55.17593 | 13869.5 | 108.25 |
| 8.873 | 29.449 | 143.7714 | 59.30554 | 13740.79 | 121.33 |
| 9.555 | 30.323 | 109.1437 | 62.21679 | 13652.02 | 223.17 |

Test Section B: rotational speed = 0 rev min$^{-1}$; air mass flow rate = $2.15 \times 10^{-3}$ kg s$^{-1}$; nominal Reynolds number = 15000.

$Bu/Ro$, there can be a reduction in the local heat transfer of about 20% compared to the stationary case. Any heat transfer design calculations for blade cooling performance which do not take cognizance of this fact could well involve regions of higher temperature than expected at the predictive stage for the leading edge. As the rotational speed is increased from zero the leading edge heat transfer initially seems to reduce in comparison to the stationary value. However for values of $Bu/Ro$ greater than about 0.005–0.01 recovery commences and the leading edge heat transfer begins to increase with increasing values of $Bu/Ro$. At sufficiently high values of $Bu/Ro$ the leading edge heat transfer could be higher than that expected when stationary. In all cases the leading edge will always be experiencing lower cooling performance compared to the trailing edge, however.

Figure 11 is intended to illustrate the complex interaction between the Coriolis and centripetal buoyancy effects. The figure does not allow easy comparison with the results of predictions made by CFD practitioners. For this reason we include the detailed results of two representative experiments in Tables 3 and 4 as a data base which may be used for predictive comparisons.

In Table 3, the input results and processed outputs are given in Test Section B (see Table 1 for geometric details) for the non-rotational case of a Reynolds number of nominally 15000 and a nominal heat flux of 29.6 kW m$^{-2}$ on the outer surface of the tube. Because of the varying external heat losses from the outer surface the actual surface heat flux varies axially and this has been allowed for in the tabulated data. It is recommended that this heat flux prescription on the outer surface is set as a boundary condition and the conjugate problem of solving for the flow and temperature fields in the fluid is combined with the simultaneous solution of the wall conduction problem. At both ends of the test section the walls may be treated as adiabatic as a first approximation. The wall temperature values quoted are results from the one-dimensional correction from the point of measurement to the effective smooth wall position as described in the earlier text.

Table 4 presents a similar set of data with the maximum rotation of 27000 rev/min and the same Reynolds number of 15000 and a nominal heat flux of 31.9 kW m$^{-2}$. This gives a nominal Rossby number of 10.5.

## 6. CONCLUSIONS

Results of an experimental investigation, aimed at examining the simultaneous effect of internal ribbing on the inside of a circular sectioned coolant channel combined with rotation of the channel, have been presented. The orientation of the channel with respect to the axis of rotation corresponds to the application of this rotating cooling passage geometry to internal cooling of gas turbine airfoil blades (i.e. orthogonal-mode rotation).

Initially experiments were conducted to establish the enhancement in heat transfer which could be expected relative to normal forced convection with smooth-walled tubes at zero rotational speed. In this respect three different rib geometries were investigated. Broadly speaking the following main conclusions have been drawn.

### 6.1. *The effect of ribs without rotation*

(1) The disruptive nature of the ribs prevents the traditional hydrodynamic and thermal boundary layer development along the tube. A mainly uniform heat flux thermal boundary condition produced a "saw tooth"-type variation of wall temperature in the downstream direction measured from the inlet of the tube. The "high" and "low" temperature regions of this "saw tooth" profile tended to occur at the rib and mid-rib locations, respectively, and a tendency for the wall temperature to generally rise in the direction of flow was observed.

(2) The variation of Nusselt number in the downstream direction reflected the "saw tooth" wall temperature distribution with the regions of relatively

Table 4. A sample of results at 2700 rev min$^{-1}$ for test section B

| Axial location, $z/D$ | Outer surface heat flux [kW m$^{-2}$] | Wall temperature on leading edge [°C] | Wall temperature on trailing edge [°C] | Fluid bulk [°C] | Local Reynolds number | Local Nusselt number on leading edge | Local Nusselt number on trailing edge | Rossby number | Buoyancy parameter on leading edge | Buoyancy parameter on trailing edge |
|---|---|---|---|---|---|---|---|---|---|---|
| 0.195 | 32.394 | 138.3 | 125.8 | 36.8 | 15007 | 118.1 | 134.7 | 9.8 | 0.328 | 0.287 |
| 1.853 | 31.336 | 168.7 | 165.6 | 44.3 | 14738 | 91.3 | 93.6 | 10.0 | 0.392 | 0.382 |
| 2.633 | 32.193 | 148.0 | 133.6 | 47.71 | 14619 | 115.2 | 134.6 | 10.1 | 0.313 | 0.267 |
| 3.412 | 31.819 | 159.4 | 147.9 | 51.2 | 14500 | 104.6 | 117.0 | 10.2 | 0.334 | 0.298 |
| 4.192 | 32.168 | 143.0 | 134.5 | 54.7 | 14385 | 128.4 | 142.1 | 10.3 | 0.269 | 0.243 |
| 4.777 | 31.794 | 146.8 | 148.3 | 57.3 | 14299 | 124.3 | 122.3 | 10.4 | 0.271 | 0.275 |
| 5.655 | 32.320 | 136.6 | 128.7 | 61.3 | 14175 | 148.6 | 165.3 | 10.5 | 0.225 | 0.203 |
| 6.435 | 31.783 | 155.8 | 149.0 | 64.8 | 14065 | 119.8 | 129.5 | 10.6 | 0.270 | 0.249 |
| 7.215 | 32.121 | 143.0 | 136.3 | 68.2 | 13959 | 146.1 | 160.5 | 10.8 | 0.219 | 0.199 |
| 7.800 | 31.505 | 162.1 | 159.2 | 70.9 | 13880 | 116.7 | 120.5 | 10.8 | 0.265 | 0.257 |
| 9.775 | 31.707 | 159.1 | 151.8 | 75.2 | 13754 | 126.3 | 138.4 | 11.0 | 0.241 | 0.220 |
| 9.355 | 32.667 | 126.3 | 115.0 | 77.8 | 13680 | 223.3 | 292.0 | 11.1 | 0.138 | 0.106 |

Test Section B: rotational speed = 2700 rev min$^{-1}$; air mass flow rate = $2.23 \times 10^{-3}$ kg s$^{-1}$; nominal Reynolds number = 15 000 and nominal Rossby number = 10.5.

"high" heat transfer occurring at the mid-rib locations. This is associated with re-attachment of the flow as observed in step-type wall flows.

(3) The presence of ribs generally improved heat transfer in the major part of the tubes tested when compared with the smooth-walled counterpart operating with the same Reynolds number based on the plain bore tube diameter.

(4) The enhancement in heat transfer over the smooth-walled situation is dependent on the rib geometry selected. It was not possible with the three rib geometries studied in this paper to fully cover all geometric variations possible. However the following broad observations are drawn. The geometries selected had an almost linear variation between the blockage ratio and the pitch : plain bore ratio and the values actually used were closely related to current cooling system design practice for gas turbine rotor blades. Within these constraints it has been demonstrated that the blockage ratio has a significant effect on the enhancement in heat transfer. To exemplify, as the blockage ratio increases from 0.36 to 0.51 to 0.64 the typical heat transfer enhancement values for all Reynolds numbers tested was respectively of the order 2.0, 2.5 and 3.0 times the smooth-walled fully developed heat transfer. To fully assess the detailed effect of other geometric features will require additional testing.

### 6.2. *The effect of ribs with rotation*

The following points highlight the main observations which emerged from the experiments undertaken with rotation of these ribbed test sections.

(1) The published work on smooth-walled cooling channels subjected to orthogonal-mode rotation has clearly illustrated that rotation influences heat transfer via two inertial mechanisms. Firstly, Coriolis forces create a cross stream secondary flow which enhances heat transfer on the trailing edge in relation to that on the leading edge of the channel. This results in the trailing edge running at a lower temperature than the leading edge. These relative changes in heat transfer over the leading and trailing edges can be modified due to the interaction of a variable coolant density and the centripetal force field. This is known as centripetal buoyancy. In general terms all these previously reported rotational effects were present with the rotating rib test sections investigated here.

(2) Rotation of the ribbed test sections demonstrated that Coriolis-induced secondary flows still affected the heat transfer on the leading and trailing edges even though it was speculated that the effect of the rib-induced flow disturbances could swamp the Coriolis effect. From the basic raw data obtained from the experiments significant differences in the leading and trailing edge temperatures were observed and these were consistent with those reported from smooth-walled tests. In this respect the leading edges were always found to run at a higher temperature for all rib geometries tested.

(3) The "saw tooth" axial variation of wall temperature was still evident with rotation although, as mentioned above, there were systematic differences between the leading and trailing edges. The corresponding axial variation in local Nusselt number was consequently similar in shape to those obtained without rotation although, obviously, the actual levels had changed. Consistent with the wall temperature measurements, the trailing edge Nusselt numbers were always higher than those on the leading edge.

(4) For a given value of Reynolds and Rossby numbers, the Nusselt numbers on the leading and trailing edges also demonstrated a sensitivity of centripetal buoyancy. On the trailing edge there was a systematic increase in Nusselt number as the buoyancy parameter increased. A similar sensitivity to buoyancy was detected on the leading edge.

(5) Uncoupling of the interaction between Coriolis forces and centripetal buoyancy has been attempted by Morris and Salemi [26] for smooth-walled coolant channels. The proposed correlating parameter involved the quotient of the buoyancy parameter and the Rossby number. This was also explored in the present investigation with ribbed channels. Although not perfect, it has been found that the rotating heat transfer performance compared to the stationary cases can be reasonably well mapped for each of the ribbed geometries tested by means of this composite rotational group.

The data presented in this paper permits an empirical assessment of the general improvement in heat transfer which may be expected by the incorporation of simple circumferential ribs onto a plain bore tube for the case of zero rotation. Additionally the graphical data presented for the rotational case permits an estimate of the likely effect of the combined effect of Coriolis forces and centripetal buoyancy to be made.

*Acknowledgements*—The authors would like to thank the Defence Research Agency and Rolls Royce, plc in the United Kingdom for the technical and financial support given during the conduct of this investigation.

## REFERENCES

1. S. N. Barua, Secondary flow in a rotating straight pipe, *Proc. R. Soc. A* **227**, 133 (1955).
2. Y. Mori and W. Nakayama, Convective heat transfer in rotating radial circular pipes (1st Report—Laminar Region), *Int. Heat Mass Transfer* **II**, 1027 (1968).
3. J. S. Benton and D. Boyer, Flow through a rapidly rotating conduit of arbitrary cross-section, *Fluid Mech.* **26** (1), 69–75 (1966).
4. H. Ito and K. Nanbu, Flow in rotating straight pipes of circular cross-section, *Trans. ASME J. Basic Engng* **93** (3), 383 (1971).
5. J. P. Johnston, R. M. Halleen and D. K. Lezius, Effects of spanwise rotation on the structure of two-dimensional fully developed turbulent channel flow, *J. Fluid Mech.* **56**, 537–557 (1972).
6. V. I. Lokai and A. S. Limanski, Influence of rotation on heat and mass transfer in radial cooling channels of turbine blades, *Izvestiya VUZ, Aviatsionnya Tekhika* **18** (3), 69 (1975).
7. D. E. Metzger and R. L. Stan, Entry region heat transfer in rotating radial tubes, *AIAA 15th Aerospace Sciences Meeting*, Los Angeles, Paper 77-189 (1977).
8. D. Skiadaressis and D. B. Spalding, Heat transfer in a pipe rotating about a perpendicular axis, ASME Paper 77-WA/HT-39 (1977).
9. L. M. Zysina-Molozken, A. A. Dergach and G. A. Kogan, Experimental investigation of heat transfer in a radially rotating pipe, *HGEEE High Temp.* **14**, 988 (1977).
10. W. D. Morris and T. Ayhan, Observations on the influence of rotation on heat transfer in the coolant channels of gas turbine rotor blades, *Proc. Instn Mech. Engng* **193** (21), 303 (1979).
11. W. D. Morris, *Heat Transfer in Rotating Coolant Channels*. Research Studies Press/John Wiley, Chichester (1981).
12. W. D. Morris and T. Ayhan, Experimental study of turbulent heat transfer in a tube which rotates about an orthogonal axis, *Proceedings of the XIV ICHMT Symposium on Heat and Mass Transfer in Rotating Machinery*, Dubrovnik, Yugoslavia, 30 August–3 September (1982).
13. R. J. Clifford, W. D. Morris and S. P. Harasgama, An experimental study of local and mean heat transfer in a triangular sectioned duct rotating in the orthogonal mode, *Proceedings of the ASME 29th International Gas Turbine Conference*, Amsterdam, Netherlands, Paper No. 84-GT-142 (1984).
14. W. D. Morris and S. P. Harasgama, Local and mean heat transfer on the leading and trailing surfaces of a square sectioned duct rotating in the orthogonal mode, Presented at *Heat Transfer and Cooling in Gas Turbines*, AGARD-CP-390, Bergen, Norway, 6–10 May (1985).
15. R. J. Clifford, Rotating heat transfer investigations on a multi-pass cooling geometry, Presented at Heat Transfer and Cooling in Gas Turbines, AGARD-CP-390, Bergen, Norway, 6–10 May (1985).
16. K. M. Iskakov and V. A. Trushin, The effect of rotation on heat transfer in the radial cooling channels of turbine blades. *Teploenergetika* **32** (2), 52–55 (1985).
17. J. H. Wagner, J. C. Kim and B. V. Johnson, Rotating heat transfer experiments with turbine airfoil internal passages, *31st International Gas Turbine Conference*, Dusseldorf, June 1986, Paper 86-GT-133 (1986).
18. W. D. Morris, S. P. Harasgama and R. Salemi, Measurements of turbulent heat transfer on the leading and trailing surfaces of a square duct rotating about an orthogonal axis, *ASME Gas Turbine and Aeroengine Congress*, Amsterdam, The Netherlands, 6–9 June (1988).
19. J. H. Wagner, B. V. Johnson and T. J. Hajek, Heat transfer in rotating passages with smooth walls and radial outward flow, *ASME Gas Turbine and Aeroengine Congress and Exposition*, 4–8 June, Toronto, Ontario, Canada (1989).
20. W. D. Morris and G. Ghavami-Nasr, Heat transfer measurements in rectangular channels with orthogonal mode rotation, *ASME Gas Turbine and Aeroengine Congress and Exposition*, 11–14 June, Brussels, Belgium (1990).
21. J. O. Medwell, W. D. Morris, J. Y. Xia and C. Taylor, An investigation of convective heat transfer in a rotating coolant channel, *ASME Gas Turbine and Aeroengine Congress and Exposition*, 11–14 June, Brussels, Belgium (1990).
22. H. Iacovides and B. E. Launder, Parametric and numerical studies of fully-developed flow and heat transfer in rotating rectangular passages, *ASME Gas Turbine and Aeroengine Congress and Exposition*, 11–14 June, Brussels, Belgium (1990).
23. J. H. Wagner, B. V. Johnson and F. C. Kopper, Heat

transfer in rotating serpentine passages with smooth walls, *ASME Gas Turbine and Aeroengine Congress and Exposition*, 11–14 June, Brussels, Belgium (1990).
24. C. Taylor, J. Y. Xia, J. O. Medwell and W. D. Morris, Finite element modelling of flow and heat transfer in turbine blade cooling, *Proceedings of European Conference on Turbomachinery*, 19–20 March, London, U.K. (1991).
25. C. Taylor, J. Y. Xia, J. O. Medwell and W. D. Morris, Numerical simulation of three-dimensional turbulent flow and heat transfer within a multi-ribbed cylindrical duct, *ASME Gas Turbine and Aeroengine Congress and Exposition*, 1–4 June, Orlando, U.S.A. (1991).
26. W. D. Morris and R. Salemi, An attempt to experimentally uncouple the effect of Coriolis and buoyancy forces on heat transfer in smooth circular tubes which rotate in the orthogonal mode, *Trans. ASME J. Turbomachinery* **114,** 858–864 (1991).
27. P. H. Rothe and J. P. Johnson, Free shear layer behaviour in rotating systems, *J. Fluids Engng* **101,** 117–120 (1979).
28. M. E. Taslim, A. Rahman and S. D. Spring, An experimental investigation of heat transfer coefficients in a spanwise rotating channel with two opposite rib-roughened walls, *ASME Gas Turbine and Aeroengine Congress and Exposition*, Toronto, Canada (1989).
29. J. H. Wagner, B. V. Johnson, R. A. Graziani and F. C. Yeh, Heat transfer in rotating serpentine passages with trips normal to the flow, *ASME Gas Turbine and Aeroengine Congress and Exposition*, 1–4 June, Orlando, U.S.A. (1991).
30. W. D. Morris and R. Salemi, The effect of orthogonal-mode rotation on forced convection in a circular-sectioned tube fitted with full circumferential transverse ribs, *Proceedings of AGARD Conference* 57, *Heat Transfer and Cooling in Gas Turbines*, Anatalya, Turkey, October (1992).
31. F. W. Dittus and L. M. K. Boelter, Calif. Pubs. Engng, Vol. 2, 1930, p. 443.